Lattice Monte Carlo Simulation for the Partitioning of a Bimodal Polymer Mixture into a Slit

Yongmei Wang*

Department of Chemistry, North Carolina Agricultural and Technical State University, Greensboro, North Carolina 27411

Iwao Teraoka

Department of Chemistry, Chemical Engineering and Material Science, Polytechnic University, 333 Jay Street, Brooklyn, New York 11201

Peter Cifra

Polymer Institute, Slovak Academy of Sciences, 842 36 Bratislava, Slovak Republic

Received June 19, 2000; Revised Manuscript Received September 5, 2000

ABSTRACT: Partitioning of a bimodal polymer mixture of different chain lengths into a narrow slit has been examined by using lattice Monte Carlo simulations in two approaches: the regular canonical ensemble simulation with a twin box and the chain insertion method. The regular canonical ensemble simulation determines the partition coefficients of the two components directly from the simulation. The results reveal that the short chains have an enhanced partitioning and the long chains have a reduced partitioning into the pore in the bimodal mixture compared with the monodisperse systems at the same concentration. In addition, the partition coefficients of the two components in the bimodal mixture maximize their difference in the semidilute concentration, substantiating the separation mechanism of the high osmotic pressure chromatography. The chain insertion method determines the chemical potentials of the chains in the bimodal mixture in the bulk and in the slit. It was found that the chemical potential depends strongly on the total volume fraction of the polymers but only weakly on the composition of the mixture in both the confined and the bulk solutions. The partition coefficients in the bimodal mixture were estimated from the chemical potentials by neglecting the dependence of the chemical potentials on the composition. The latter produced a less pronounced enhancement and reduction in the partition coefficients of the two components compared with those obtained from the simulations using the twin box.

I. Introduction

Teraoka and co-workers have recently tapped into the chromatographic methods that make use of the equilibration of semidilute and concentrated solutions with porous media. They developed techniques known as high osmotic pressure chromatography (HOPC) for large-scale fractionation[1] of polydisperse polymers by the molecular weight and phase fluctuation chromatography (PFC) for separation of random block copolymers by their chemical compositions.[2] In HOPC, polydisperse polymers are dissolved in a good solvent at high concentrations and injected into chromatographic columns that are packed with porous materials with a pore size comparable to the size of the polymers. It was theoretically suggested[3,4] that the high osmotic pressure in the semidilute solution drives the low molecular weight components (LMWC) into the confined media preferentially. The solution in the pore is enriched with the LMWC whereas the solution in the exterior region is enriched with the high molecular weight components (HMWC). This enhanced partitioning of the LMWC in the confined media facilitates the fractionation of polydisperse polymers. Teraoka and co-workers have demonstrated the performance of HOPC to be superior to that of the conventional size exclusion chromatography used for the purpose of fractionation.[5,6] Furthermore, HOPC consumes less solvent and therefore is more environmentally benign.

The partitioning of a bimodal mixture of polymers with different molecular weights in semidilute solutions illustrates the principle of HOPC. Teraoka et al. investigated the partitioning of a bimodal mixture polymers both experimentally and theoretically.[3,7−9] They developed a theory[3] that determines the partition coefficients for a monodisperse sample and a bimodal mixture in a wide range of concentrations. The theory uses the dependence of the osmotic pressure on the concentration and composition derived in the renormalization group theory. For the monodisperse solution, the theory predicts an increase in the partition coefficient K as the external concentration ϕ increases and $K \to 1$ as $\phi \to 1$. For the bimodal mixture, the theory[3] predicts a strongly enhanced partitioning of the LMWC into the pore and the occurrence of the partitioning inversion for the LMWC ($K_L > 1$). The partition coefficient of the LMWC can easily be much greater than one according to the theory. On the basis of the theoretical calculations, Teraoka et al. developed the enhanced partitioning fractionation (EPF)[10] and eventually the HOPC for large-scale chromatographic separation.[1]

Experimentally, Teraoka et al. used the space-resolved Jamin interferometry to study the penetration of the pore by the monodisperse samples.[7] The partition coefficient of the monodisperse sample showed a weak-to-strong penetration transition as the exterior bulk concentration increased. The partition coefficients were comparable with the theoretical calculations. Penetra-

10.1021/ma001074y CCC: $20.00
Published on Web 12/08/2000

tion of the pore by the bimodal mixture was studied directly in EPF.[8] The concentrations of the two polymers exterior to the pore showed an oscillatory behavior. The partition coefficient of the LMWC much greater than one was observed. The experimental results were, however, subjected to large errors. A comparison between the experimental results and the theory was not made.

Computer simulations can provide unambiguous results. Comparison between simulation results and theory can provide a rigorous test of the theory. Earlier computer simulation studies of the partitioning, however, primarily focused on the partitioning in the dilute solution limit.[11] Cifra et al. examined the first- and second-order dependence of the partition coefficient on the concentration.[12,13] Yethiraj and Hall studied the equilibrium partitioning of chain fluids between a bulk and a pore using off-lattice Monte Carlo simulations.[14,15] They used a simulation box consisting of a pore region and a bulk region, similar to the one adopted here. The polymer chains studied were short oligomers, and the solvent particles were absent. Therefore, the partitioning studied differs from the partitioning of a polymer solution into a pore. Recently, Wang and Teraoka performed lattice Monte Carlo simulations for the partitioning of monodisperse polymer solutions for a wide range of concentrations.[16] The weak-to-strong penetration transition was clearly observed. The comparison between the simulation results and the theory by Teraoka et al. reveals some deficiencies in the theory. The theoretical results fit the simulation results reasonably only when the empirical results on the confinement energy determined in the simulations were used by the theory. Even then the two agreed qualitatively but not quantitatively. For the partitioning of the bimodal mixture, the theory further relies on a result derived by the renormalization group theory that has not been rigorously tested. The theoretical prediction of a large partition coefficient much greater than one for the LMWC at high concentrations is doubtful. A clear understanding on the partitioning of the bimodal mixture especially at semidilute region is still lacking.

Here, we report the lattice Monte Carlo simulations for the partitioning of the bimodal mixture. Two different simulation techniques were employed: the regular canonical ensemble simulation and the chain insertion method. The canonical ensemble simulation examines the equilibration in a solution of the bimodal mixture between a bulk and a confined slit. The partition coefficients were obtained from the average densities of each component in the two regions. Partitioning inversion was observed for the short chains, but the partition coefficient for the short chains is only slightly above one at high concentrations. The results were discussed in light of the chromatographic separation in HOPC. The chain insertion method permits the determination of the chemical potential of a polymer chain in a solution of a polymer mixture. Our study shows that the chemical potential depends primarily on the total volume fraction of the two polymers and that the influence of the mixture composition on the chemical potential is small both in the confined solution and in the bulk. We were then able to estimate the partition coefficients of the bimodal mixture from the chemical potentials. The partition coefficients thus determined agree qualitatively but not quantitatively with the partition coefficients determined directly from the canonical ensemble simulation. The latter results are more reliable.

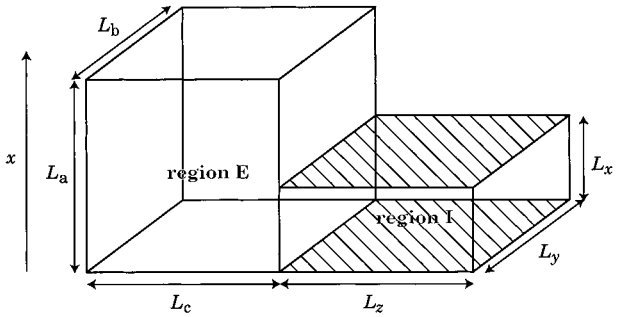

Figure 1. Schematic drawing of the simulation box.

Table 1. Size of Polymer Chains Used in the Simulations

N	$2R_g$	ϕ^* [a]
25	5.52	0.341
100	13.0	0.116
400	29.4	0.0425

[a] The overlap concentration ϕ^* was estimated from $(\phi^*/N)[2^{1/2}(R_g+\alpha)]^3 = 1$, where $\alpha = 0.199$ accounts for the thickness of a coating needed to translate the volume on the lattice into the volume occupied by the chain in the continuous space (see ref 25).

II. Simulation Method

A. Regular Canonical Ensemble Simulation. The regular canonical ensemble simulation was performed with a twin box as shown in Figure 1. Details of the simulation method were reported earlier.[16] The important features of the simulation box are briefly described here. The simulation box is a simple cubic lattice that has two connected regions: region E representing the exterior bulk solution and region I representing the interior pore channel. There are two solid walls extending in the y and z directions in region I. No polymer beads may occupy the sites on the wall. The distance between the two walls can be varied to represent different widths of the pore channel. Periodic boundary conditions (PBC) are applied in all of the three directions except where the walls are. For the simulations reported here, the typical box size used was $30 \times 30 \times 50$ for region E and $(D + 1) \times 30 \times 50$ for region I where D is the slit width. The volume of region E (V_E) is always larger than the volume of region I (V_I), typically about 5 times as large. The condition of $V_E \gg V_I$ will ensure that the composition of the exterior solution does not change appreciably during the equilibration.

There are two types of homopolymer chains in the simulation box, namely, type L with chain length of N_L and type H with chain length N_H ($N_L < N_H$). Table 1 lists the size of chains used in the simulations. No interactions were applied between the segments of L and H chains or between the segments and the wall except the excluded-volume interaction. Initially polymer chains were placed randomly in the bulk region using the chain insertion method. The system was then equilibrated by using the reptation moves with the Metropolis rule. Some of the chains migrated into the pore and established an equilibrium. After the equilibration, average density profiles along the x direction of both components were collected in both regions (a total of four density profiles were collected). The layers near the edge where the two regions meet were excluded from obtaining the average density profiles. Typically, the number of layers excluded was slightly larger than

the radius of gyration of the longer chains. This simulation method was employed in the earlier study for the partitioning of the monodisperse solution in the concentration range from dilute to concentrated.[16] Simulation for the partitioning of the bimodal mixture using the same method, however, requires a much longer equilibration time than the time required for the monodisperse solution. The equilibration is primarily determined by the rate of exchange of chains between the bulk and the confined regions. The highest volume fraction of the polymers in the bulk region investigated is around 0.5. The corresponding concentration in the pore is lower than that. The equilibration of polymer systems at these concentrations do not pose problems. The smoothness of the density profiles collected in the bulk and pore regions is used as a measure of sufficiency of the equilibration time used for the system.

The four density profiles give rise to four average concentrations: ϕ_L^I, ϕ_L^E, ϕ_H^I, ϕ_H^E, the volume fractions of components L and H in region I and region E, respectively. Three partition coefficients are defined as follows.

$$K_L = \phi_L^I/\phi_L^E \quad (1)$$

$$K_H = \phi_H^I/\phi_H^E \quad (2)$$

$$K_{tot} = \phi^I/\phi^E \quad (3)$$

where $\phi^I = \phi_L^I + \phi_H^I$ and $\phi^E = \phi_L^E + \phi_H^E$. The physical meanings of K_L and K_H are self-evident. They are the partition coefficients of component L and H, respectively. K_{tot} is the partition coefficient of the total polymer segments including both types and will be named as the segmental partition coefficient.

B. Chain Insertion Method. The chain insertion method is an extension of the Widom particle insertion method and has been used widely in the study of polymeric systems.[17−21] The chain insertion method was used to determine the chemical potential of a chain in the bulk solution and in the confined solution. A test chain of a given length can be inserted in a configuration of the polymer solution generated by the regular canonical ensemble simulation with a lattice that contains only region E for the bulk solution and only region I for the confined solution. A Rosenbluth weighting factor, w_i, is determined for each grown segment: $w_i = Z_i/(Z - 1)$, where Z_i is the number of empty lattice sites available during the insertion of the ith segment and Z is the number of nearest lattice sites ($Z = 6$ in the simple cubic lattice). The chemical potential of the inserted chain $\beta\mu$, with reference to a nonreverse random walk chain on the same lattice, is given by

$$-\beta\mu = \ln\langle(1 - \phi)\prod_{i=2}^{N} w_i\rangle \quad (4)$$

where β is the reciprocal of the thermal energy and ϕ is the volume fraction of the polymer segments in the solution. The ensemble average is taken by averaging μ over different trials of insertion of the test chain in a number of different configurations of the polymer solution. In this study, the inserted chains can have two different chain lengths, N_L and N_H. The chemical potentials thus determined are μ_L and μ_H, which are a function of the total volume fraction and the composition of the mixture. Let μ_H^I, μ_L^I, μ_H^E, and μ_L^E be the chemical potentials of type H and type L chains in the confined solution and in the bulk solution, respectively. Then, the partition coefficients K_H and K_L for the partitioning of the bimodal mixture can be estimated by solving the following equations

$$\mu_H^I(\phi^I,P_H^I)/k_BT + \ln(\phi^I P_H^I) = \mu_H^E(\phi^E,P_H^E)/k_BT + \ln(\phi^E P_H^E) \quad (5)$$

$$\mu_L^I(\phi^I,P_H^I)/k_BT + \ln(\phi^I(1 - P_H^I)) = \mu_L^E(\phi^E,P_H^E)/k_BT + \ln(\phi^E(1 - P_H^E)) \quad (6)$$

where $P_H^I = \phi_H^I/\phi^I$ and $P_H^E = \phi_H^E/\phi^E$ give the compositions of the confined and the bulk solution, respectively. The μ defined in eq 4 does not include the term for the entropy of mixing; therefore, one needs to include the term when equating the chemical potentials in the bulk and confined regions that have different concentrations.

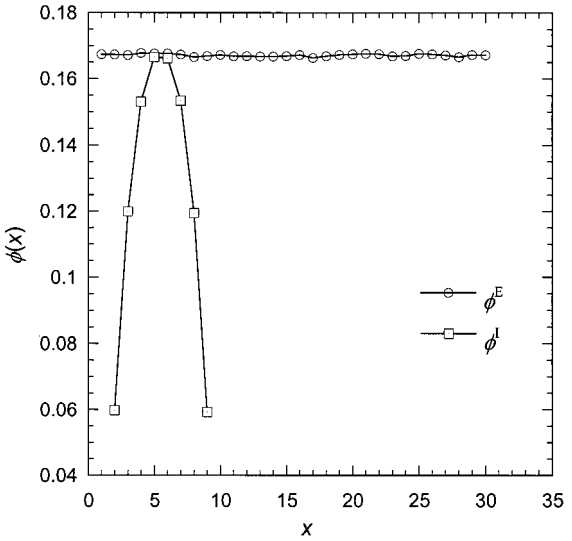

Figure 2. Segmental density profiles along the x-direction in region E and region I for the partitioning of a monodisperse solution of a chain length $N = 25$ into a slit of width $D = 9$. The simulation box used was $30 \times 30 \times 50$ for region E and $10 \times 30 \times 50$ for region I.

III. Results and Discussion

A. Partition Coefficient from the Canonical Ensemble Simulation. We first present the density profiles that demonstrate the partitioning inversion of short chains in the bimodal mixture. Figure 2 shows the typical density profiles in region I and region E for the partitioning of a monodisperse solution ($N = 25$, $D = 9$, $\phi^E = 0.168$). The density profile is flat in region E and is bell-shaped in region I. The peak density in region I is lower than or equal to the density in region E at all concentrations. This is no longer the case in the partitioning of the bimodal mixture. Figure 3 presents the density profiles of the two components in both regions for the partitioning of a solution of the bimodal mixture with equal volume fractions. The two chain lengths used are $N_H = 100$ and $N_L = 25$, and the slit width is $D = 9$. The peak density of the short chains in region I is much higher than it is in region E, an indication of the partitioning inversion of the short chains in the slit. The average density of short chains in the slit, ϕ_L^I, is however not necessarily greater than ϕ_L^E. In contrast,

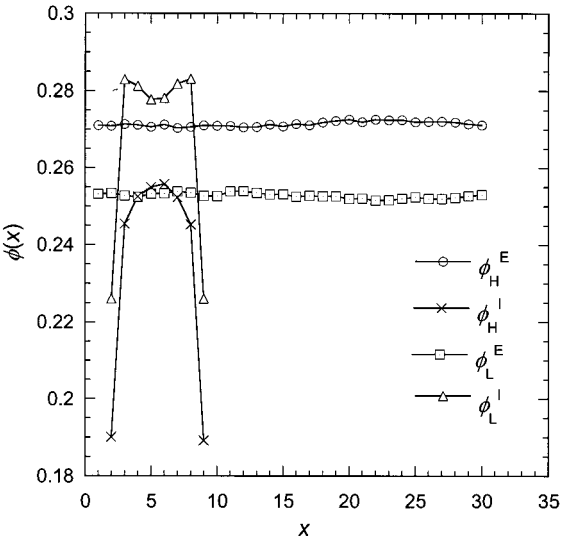

Figure 3. Segment density profiles along the x-direction in region E and region I for the partitioning of a bimodal mixture, $N_H = 100$, $N_L = 25$ into a slit of width $D = 9$. The simulation box used was the same as in Figure 2.

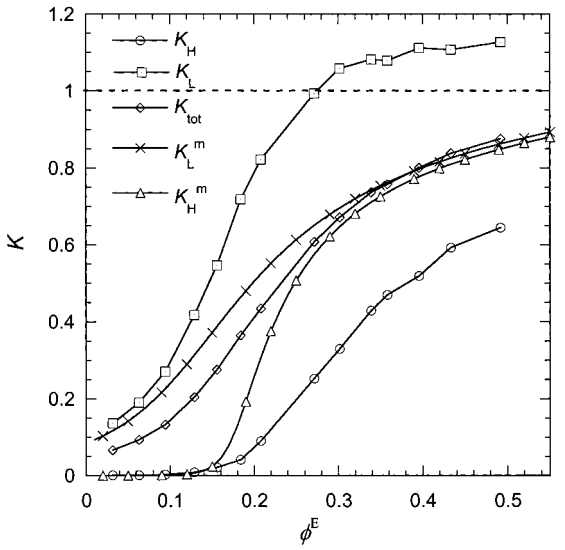

Figure 4. Partition coefficients, K_H, K_L, and K_{tot}, of a bimodal mixture plotted as a function of the total exterior bulk concentration, ϕ^E, along with K_H^m and K_L^m for the monodisperse samples. $N_H = 100$, $N_L = 25$, $D = 5$.

the peak density of the long chains in the slit ϕ_H^I is always less than ϕ_H^E.

Figure 4 presents three partition coefficients, K_H, K_L, and K_{tot}, in the partitioning of a bimodal mixture ($N_H = 100$, $N_L = 25$, $D = 5$) as a function of the total exterior concentration ϕ^E. In the bimodal mixture, K_L and K_H will depend on the concentration as well as the composition of the exterior solution. Here, the composition of the exterior solution before the equilibration was exactly 50% and after the equilibration was 51−53% in the longer chains. Hence, the bulk solution may be considered as a reservoir of a equal-volume mixture at the given concentration. The figure also includes the partition coefficients of the monodisperse samples, K_L^m and K_H^m, of the two components as a function of the bulk concentration. At low concentrations, K_L and K_H are close to K_L^m and K_H^m, respectively, a reasonable result since the interchain interactions can be neglected in the dilute solutions. At high concentrations, the short chains

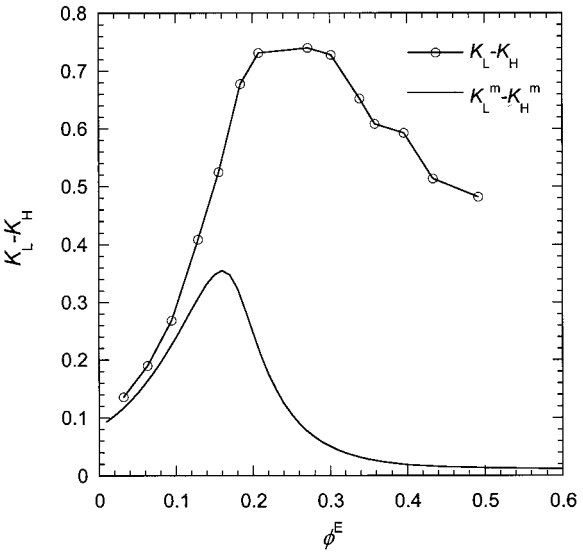

Figure 5. Plot of $K_L - K_H$ and $K_L^m - K_H^m$ as a function of ϕ^E for the same system as in Figure 4.

now have an enhanced probability to enter the slit than those in the monodisperse solution ($K_L > K_L^m$), and the long chains have a reduced probability to enter the slit ($K_H < K_H^m$). The segmental partition coefficient K_{tot} is between K_L^m and K_H^m and $K_{tot} \to 1$ as $\phi^E \to 1$. K_H and K_L, however, do not approach unity as $\phi^E \to 1$. The latter can be expected when one considers a melt of a bimodal mixture confined in a slit. In the melt, $K_{tot} = 1$, since there will be no void in both the bulk and the confined regions. However, in a confined athermal melt of a mixture short chains are known to segregate to the walls since the short chains experience a smaller entropy loss near the walls than the longer chains do.[22] Such surface segregation of the short chains can also been seen from the density profiles in Figure 3. The profile for the short chain in region I is no longer bell-shaped but has two peaks near the walls. The density near the walls is higher than that in the middle of the slit. In the confined melt, the long chains will be depleted, and the short chains will be enhanced near the walls. Hence, $K_H < 1$ and $K_L > 1$ in the partitioning of the bimodal mixture in the limit of $\phi^E = 1$. The magnitude of deviation of K_H and K_L from the unity will depend on the chain lengths N_H and N_L and the slit width D.

In the column chromatography, the difference in K_L and K_H gives a measure for the separation between the two components of H and L. Figure 5 presents $K_L - K_H$ in the bimodal mixture and $K_L^m - K_H^m$ for the monodisperse sample for the same system as in Figure 4. One sees $K_L^m - K_H^m$ has a maximum at $\phi^E \approx 0.16$. The physical explanation for the presence of the maximum in $K_L^m - K_H^m$ is as follows. In the partitioning of a monodisperse sample, the partition coefficient increases as the bulk concentration increases. The increase is significant when the correlation length in the bulk solution becomes smaller than the slit width. In the system studied here, the slit width is comparable with the size of the short chains ($D \approx 2R_g$) but smaller than the size of the long chains. Therefore, as ϕ increases, K_L^m increases significantly, but K_H^m does not increase significantly until ϕ^E is sufficiently high such that the correlation length in the solution of long chains is smaller than the slit width. Hence, the difference $K_L^m -$

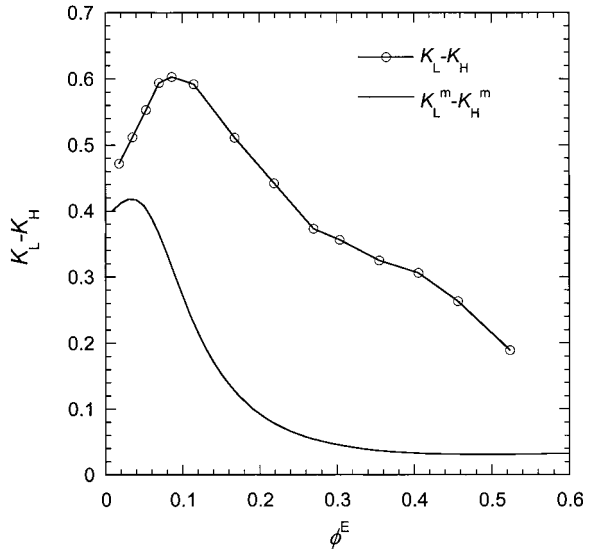

Figure 6. Plot of $K_L - K_H$ and $K_L^m - K_H^m$ as a function of ϕ^E for the partitioning of a bimodal mixture, $N_H = 100$ and $N_L = 25$ into a slit of width $D = 9$.

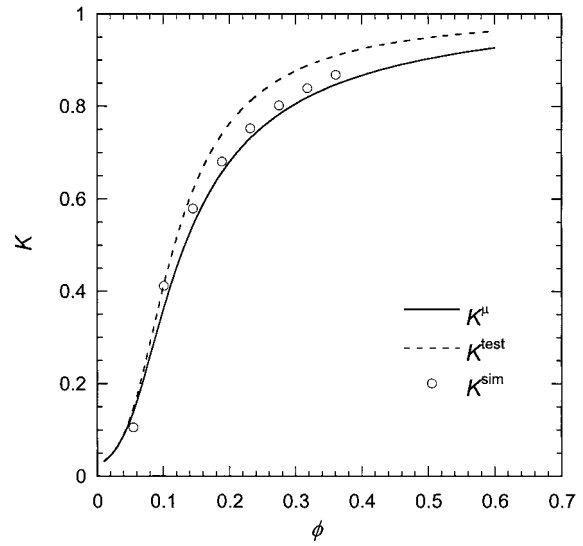

Figure 7. Comparison of K^{sim} obtained in the canonical ensemble simulation in the twin box with K^μ and K^{test} for the partitioning of a monodisperse sample of $N = 100$ into a slit of width $D = 9$.

K_H^m will show a peak at the concentration where K_H^m begins to increase significantly (the weak-to-strong penetration transition).[23,24] In the bimodal mixture, $K_L - K_H$ differs even more, and its peak is broadened and shifted to the right. In addition, $K_L^m - K_H^m$ goes to zero as $\phi^E \to 1$, but $K_L - K_H$ is nonzero at $\phi^E = 1$, as explained earlier. More investigations are needed to understand the characteristics of the peak in $K_L - K_H$ in the bimodal mixture. The presence of the peak in $K_L - K_H$ at semidilute concentration however substantiates the separation mechanism in HOPC. The separation of the two components can be achieved in the semidilute range where K_L and K_H differ most. Furthermore, there is a wide range of concentrations where $K_L - K_H$ stays at high values. This indicates that the separation of the two components remains good in a wide range of concentrations. Earlier experimental and theoretical studies have not identified this important feature.

Figure 6 presents a similar plot of $K_L - K_H$ vs ϕ^E for the same mixture of $N_H = 100$ and $N_L = 25$ but with a broader slit of $D = 9$. The same feature as in Figure 5 is observed in Figure 6. The peak, however, is shifted to a lower ϕ^E, and the peak height is lower. Apparently, an increase in D reduces the difference in K_L and K_H and lowers the performance of the separation. Nevertheless, the enhancement of $K_L - K_H$ in the bimodal mixture is evident compared with the monodisperse counterpart. For this particular combination of N_H and N_L, we are not able to examine a smaller D. Simulations on other systems are being carried out to examine the optimum choice of D for a given combination of chain lengths.

Teraoka et al.[3] formulated a mean-field theory that calculates the partitioning coefficients of a bimodal polymer mixture of different chain lengths. The theory used the dependence of the osmotic pressure on the volume fraction and the composition for a polydisperse polymer solution obtained by Ohta and Oono[26] using the renormalization group theory. Comparison between the theory and the simulation results (not shown) reveals that the theory has some deficiencies. The theoretical result of $K_L - K_H$ is much larger compared at the same ϕ^E, and the peak is shifted to a much higher ϕ^E. The theory is not able to give a reasonable prediction about the partitioning of the bimodal mixture. Theoretical understanding of the thermodynamics of a bimodal mixture is far from satisfactory. Below we present results on the chemical potentials for the bimodal mixture in an attempt to understand the partitioning results for the bimodal mixture.

B. Partition Coefficient from the Chain Insertion Method. In an earlier study we used the chain insertion method to determine μ^I and μ^E as a function of ϕ for the monodisperse solutions in confined regions and in bulk.[25] Equating μ^1 and μ^E, we can estimate the partition coefficient K^μ for the monodisperse sample:

$$\ln \phi^I + \mu^I(\phi^I)/k_B T = \ln \phi^E + \mu^E(\phi^E)/k_B T \qquad (7)$$

We solved the above equation numerically to obtain $K^\mu = \phi^I/\phi^E$ as a function of ϕ^E. As discussed in our earlier paper, the dependences of μ^E and μ^I on ϕ are similar regardless of the slit width. Therefore, we can evaluate the partition coefficient K^{test} by replacing $\mu^I(\phi)$ with $\mu^E(\phi) + \Delta\mu_0$, where $\Delta\mu_0 = \mu^I(0) - \mu^E(0)$ is the difference in the chemical potential between the confined solution and the bulk solution in the zero concentration limit. The latter method eliminates the need to evaluate the dependence of μ^I on ϕ^I for each slit width. Figure 7 compares K^μ and K^{test} along with the partition coefficient K^{sim} determined directly from the canonical ensemble simulation. K^μ agrees with K^{sim}, and both are slightly lower than K^{test} at high concentrations. The difference, however, is small, and the results depend sensitively on $\mu^I(\phi)$ and $\mu^E(\phi)$. The small difference between K^μ and K^{test} justifies the use of $\mu^E(\phi) + \Delta\mu_0$ for $\mu^I(\phi)$ in order to estimate K for the monodisperse sample.

In the bimodal mixture, μ_H and μ_L now depend on the concentration ϕ and the composition P_H. Chain insertion method is used again to examine how μ_H and μ_L depend on ϕ and P_H for the bulk and the confined solutions. Figure 8a presents $\mu_L^E(\phi,P_H)$ and $\mu_L^I(\phi,P_H)$ at two compositions, $P_H = 0$ and $P_H = 0.5$, for a bimodal mixture of $N_H = 100$ and $N_L = 25$, $D = 9$ for the confined solution. One can see $\mu_L(\phi,0.5)$ and $\mu_L(\phi,0)$ are almost indistinguishable from each other both for the bulk solution and for the confined solution. The same is true

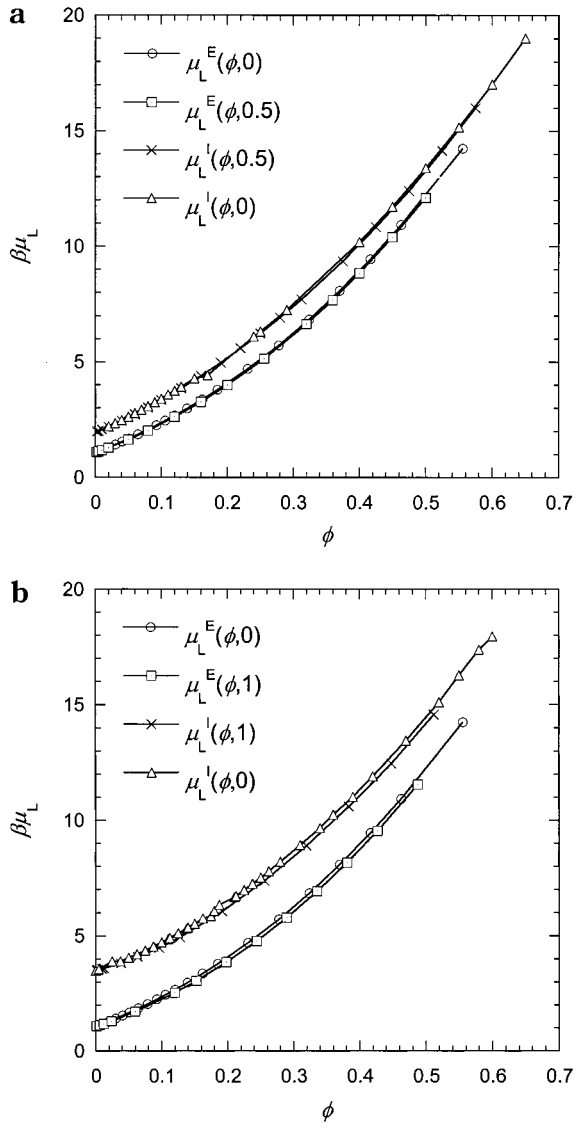

Figure 8. Plots of μ_L vs ϕ for a solution of bimodal mixture in the bulk solution and in a confined solution of slit width $D = 9$ at different compositions: (a) $N_H = 100$, $N_L = 25$, $P_H = 0$ and 0.5; (b) $N_H = 400$, $N_L = 25$, $P_H = 0$ and 1.

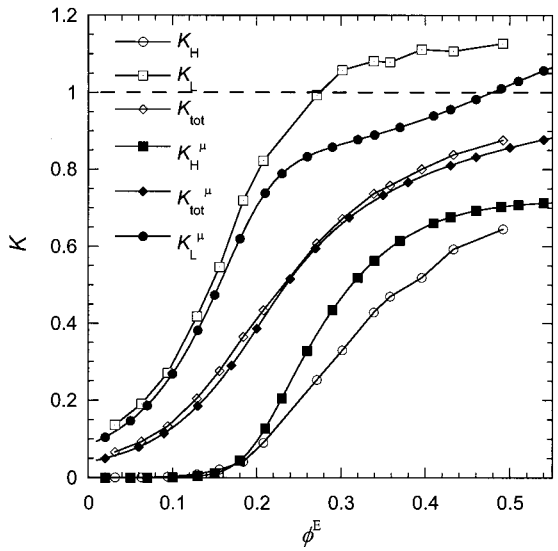

Figure 9. Comparison between K_H, K_L, and K_{tot} obtained directly from the canonical ensemble simulation using the twin box with K_H^μ, K_L^μ, and K_{tot}^μ for the partitioning of a bimodal mixture of the same system as in Figure 4.

for μ_H (not shown). Similar results were obtained for other combinations of chain lengths such as $N_H = 400$ and $N_L = 25$. Only $\mu_L(\phi,0)$ and $\mu_L(\phi,1)$ slightly differ from each other at intermediate concentrations. Figure 8b presents $\mu_L^E(\phi,P_H)$ and $\mu_L^I(\phi,P_H)$ at $P_H = 0$ and 1 for a mixture of $N_H = 400$ and $N_L = 25$. One finds $\mu_L(\phi,0) > \mu_L(\phi,1)$ for both solutions. This means that the chemical potential of a short chain μ_L is slightly lower in a solution of long chains than it is in a solution of short chains at the same volume fraction. Likewise, one finds the chemical potential of a long chain μ_H is slightly higher in a solution of short chains than it is in a solution of long chains (not shown). The difference, however, is small at least in the range of chain lengths studied here. The more uniform distribution of segments in a solution of short chains compared with that in a solution of long chains at the same volume fraction is more effective in blocking the insertion of a test chain of either length. There is also an indication in Figure 8 that the chemical potentials in the confined solution depend on the composition slightly more sensitive than those in the bulk solution do. This can be expected since the confined solution has some inhomogeneity in densities near the walls. The above result is in partial agreement with the scaling law picture. In the scaling theory, the chemical potential of a chain should only depend on the volume fraction of the polymers in semidilute solutions and not the composition.

On the basis of the above results, one may assume that μ_H^I, μ_L^I, μ_H^E, and μ_L^E are insensitive to the composition. One can therefore use the chemical potentials determined for the monodisperse solutions to solve eqs 5 and 6. We solved eqs 5 and 6 for ϕ^I and P_H^I as a function of ϕ^E at $P_H^E = 0.5$. The three partition coefficients defined for the bimodal solution were obtained correspondingly, $K_H^\mu = \phi^I P_H^I/(\phi^E P_H^E)$, $K_L^\mu = \phi^I(1 - P_H^I)/[\phi^E(1 - P_H^E)]$, and $K_{tot}^\mu = \phi^I/\phi^E$. Figure 9 presents the calculated K_H^μ, K_L^μ, and K_{tot}^μ for the system studied in Figure 4, along with the data obtained directly in the canonical ensemble simulations using the twin box. The calculated K_L^μ, K_H^μ, and K_{tot}^μ possess the same feature as K_L, K_H, and K_{tot} determined directly in the simulation. K_{tot}^μ agrees well with K_{tot} for the whole range of concentrations studied, but $K_H^\mu > K_H$ and $K_L^\mu < K_L$ at high concentrations. The agreement between K_i^μ and K_i (i = L, H) is worse in the bimodal mixture compared with the one in Figure 7 for the monodisperse samples. The larger discrepancy is ascribed to the dependence of μ on P_H neglected in solving eqs 5 and 6. Apparently, the chemical potentials of the chains in the bimodal mixture depend on the composition even though the dependence is weak, and this weak dependence influences the enhancement of the short chains in the pore at high concentrations.

The comparison between K^μ and K obtained directly from the canonical ensemble simulation reveals that the direct estimation of K from the simulation using the twin box is preferred especially in the partitioning of the bimodal mixture. This situation is similar to the one encountered in the estimation of phase equilibria based on the calculation of chemical potentials or the direct estimation of the phase coexistence in the Gibbs ensemble.[20] In the latter case, the Gibbs ensemble method is also preferred. The difference between our twin box simulation and the Gibbs ensemble method is that there

is a direct contact between the slit and the unconfined solution in the former, whereas in the Gibbs ensemble the two phases in equilibrium are not in direct contact. In the partitioning of polymer solutions, the contact between exterior and interior solutions is well-defined and does not have problems such as broad and fluctuating interfaces between coexisting phases that make the exchange of chains difficult.

IV. Conclusion

The partitioning for a solution of a bimodal polymer mixture differing in chain length into a slit has been studied by using lattice Monte Carlo simulations. The enhancement of the short chains in the slit is clearly observed. Several other features of the partitioning of the bimodal mixture can be summarized here. First, $K_{tot} \rightarrow 1$ as $\phi \rightarrow 1$, but K_L remains above K_{tot} and K_H remains below K_{tot}. This is due to the surface segregation of the short component in the slit. Partitioning inversion of the short component is observed at high concentrations, but the enhancement of the short chains in the pore is not as great as that predicted by the earlier theory. Second, $K_H - K_L$ shows a maximum at a semidilute concentration when plotted as a function of ϕ^E. This peak is likely the key factor that determines the separation in HOPC. Earlier studies have not identified this important feature. More investigations will be carried out to understand the characteristics of the peak. Furthermore, one finds that the chemical potentials of the long and short chains in the mixture depend strongly on the total volume fraction of the polymers but weakly on the composition. The enhancement of the short component in the pore can be reproduced to a certain degree by neglecting the dependence of the chemical potentials on the composition. An accurate prediction, however, would require the consideration of the dependence of the chemical potentials on the composition.

Acknowledgment. This research is supported by NSF (DMR-9876360) and the Petroleum Research Fund (PRF-32707-GB5). We also acknowledge the computer resource support provided by the North Carolina Super Computer Center. P.C. acknowledges the support of this work by Grant Agency for Science (VEGA) Grant 2/7076/20.

References and Notes

(1) Luo, M.; Teraoka, I. *Macromolecules* **1996**, *29*, 4226−4233.
(2) Xu, Y.; Teraoka, I. *Macromolecules* **1998**, *31*, 4143−4148.
(3) Teraoka, I.; Zhou, Z.; Langley, K. H.; Karasz, F. E. *Macromolecules* **1993**, *26*, 3223−3227.
(4) Teraoka, I.; Zhou, Z.; Langley, K. H.; Karasz, F. E. *Macromolecules* **1993**, *26*, 6081−6085.
(5) Xu, Y.; Teraoka, I.; Senak, L.; Wu, C.-S. *Polymer* **1999**, *40*, 7359−7366.
(6) Dube, A.; Teraoka, I. *Isol. Purif.* **1999**, *3*, 51−63.
(7) Dube, A.; Teraoka, I. *Macromolecules* **1997**, *30*, 5352−5360.
(8) Dube, A.; Teraoka, I. *Macromolecules* **1997**, *30*, 7753−7758.
(9) Teraoka, I. *Macromolecules* **1996**, *29*, 2430−2439.
(10) Dube, A.; Teraoka, I. *Macromolecules* **1995**, *28*, 2592−2595.
(11) Teraoka, I. *Prog. Polym. Sci.* **1996**, *21*, 89−149.
(12) Cifra, P.; Bleha, T.; Romanov, A. *Makromol. Chem., Rapid Commun.* **1988**, *9*, 355−359.
(13) Bleha, T.; Cifra, P.; Karasz, F. E. *Polymer* **1990**, *31*, 1321−1327.
(14) Yethiraj, A.; Kall, C. K. *J. Chem. Phys.* **1989**, *91*, 4827−4837.
(15) Yethiraj, A.; Hall, C. K. *Mol. Phys.* **1991**, *73*, 503−515.
(16) Wang, Y.; Teraoka, I. *Macromolecules* **1997**, *30*, 8473−8477.
(17) Rosenbluth, M. N.; Rosenbluth, A. W. *J. Chem. Phys.* **1955**, *96*, 2395−2401.
(18) Frenkel, D.; Mooju, G. C. A. M.; Smit, B. *J. Phys.: Condens. Matter* **1992**, *3*, 3053−3058.
(19) Pablo, J. J.; Laso, M.; Suter, U. W. *J. Chem. Phys.* **1992**, *96*, 6157−6163.
(20) Macki, A. D.; Panagiotopoulos, A. Z.; Kumar, S. K. *J. Chem. Phys.* **1995**, *102*, 1014−1023.
(21) Frenkel, D.; Smit, B. *Understanding Molecular Simulation: From Algorithms to Applications*; Academic Press: San Diego, 1996.
(22) Hariharan, A.; Kumar, S. K.; Russell, T. P. *Macromolecules* **1990**, *23*, 3584−3592.
(23) Daoud, M.; De Gennes, P. G. *J. Phys. (Paris)* **1977**, *38*, 85.
(24) de Gennes, P. G. *Scaling Concepts in Polymer Physics*; Cornell University Press: Ithaca, NY, 1996.
(25) Wang, Y.; Teraoka, I. *Macromolecules* **2000**, *33*, 3478−3484.
(26) Ohta, T.; Oono, Y. *Phys. Lett.* **1982**, *89A*, 460−464.

MA001074Y